PCCP

PAPER

Cite this: *Phys. Chem. Chem. Phys.*, 2014, **16**, 21330

Symmetry-breaking in the endofullerene $H_2O@C_{60}$ revealed in the quantum dynamics of *ortho* and *para*-water: a neutron scattering investigation

Kelvin S. K. Goh,[a] Mónica Jiménez-Ruiz,[b] Mark R. Johnson,[b] Stéphane Rols,[b] Jacques Ollivier,[b] Mark S. Denning,[c] Salvatore Mamone,[c] Malcolm H. Levitt,[c] Xuegong Lei,[d] Yongjun Li,[d] Nicholas J. Turro,†[d] Yasujiro Murata[e] and Anthony J. Horsewill*[a]

Received 23rd July 2014,
Accepted 22nd August 2014

DOI: 10.1039/c4cp03272a

www.rsc.org/pccp

Inelastic neutron scattering (INS) has been employed to investigate the quantum dynamics of water molecules permanently entrapped inside the cages of C_{60} fullerene molecules. This study of the supramolecular complex, $H_2O@C_{60}$, provides the unique opportunity to study isolated water molecules in a highly symmetric environment. Free from strong interactions, the water molecule has a high degree of rotational freedom enabling its nuclear spin isomers, *ortho*-H_2O and *para*-H_2O to be separately identified and studied. The INS technique mediates transitions between the *ortho* and *para* spin isomers and using three INS spectrometers, the rotational levels of H_2O have been investigated, correlating well with the known levels in gaseous water. The slow process of nuclear spin conversion between *ortho*-H_2O and *para*-H_2O is revealed in the time dependence of the INS peak intensities over periods of many hours. Of particular interest to this study is the observed splitting of the ground state of *ortho*-H_2O, raising the three-fold degeneracy into two states with degeneracy 2 and 1 respectively. This is attributed to a symmetry-breaking interaction of the water environment.

I. Introduction

The encapsulation of a water molecule inside the cage of a C_{60} fullerene provides a unique opportunity to study H_2O in a highly symmetrical, homogenous and isolated environment. In its cage, free from hydrogen bonding and other strong interactions, the water molecule possesses a high degree of rotational freedom providing an important pre-requisite for investigating its quantum dynamical behaviour, including its rotation and important properties associated with its nuclear spin isomers, *ortho* and *para*-water.

The entrapment of the water molecule inside a fullerene was innovated in 2011 by the group of Murata[1] using the 'molecular surgery' techniques he pioneered in collaboration with Komatsu.[2] In a series of chemical reactions, an orifice is opened in a C_{60} cage and stabilised with attached groups. A small molecule, H_2O in this case, is inserted through the orifice at high temperature whereupon it becomes trapped inside the cage. A further series of chemical reactions seals the orifice to yield the endofullerene $H_2O@C_{60}$. The resulting supramolecular complex provides a 'nanolaboratory' environment[3] in which the quantum rotor, H_2O, can be investigated using various forms of spectroscopy. The first such physical investigation of $H_2O@C_{60}$ was undertaken in 2012 at low temperature using three forms of spectroscopy; far-infrared, inelastic neutron scattering (INS) and solid state nuclear magnetic resonance (NMR).[4] Analogous to earlier investigations on other small molecule endofullerenes such as $H_2@C_{60}$,[5–16] these first experiments revealed the quantum rotation of the water molecule and conclusively identified its nuclear spin-isomers, *ortho*-H_2O and *para*-H_2O, in the various spectra. The existence of these two species is founded in the requirement for the total wavefunction of the water molecule to be anti-symmetric upon exchange of two fermions, in this case the two ^1H nuclei. The *para* spin-isomer has total nuclear spin $I = 0$ and is the ground state of H_2O while *ortho*-H_2O has $I = 1$. Being a process involving space and spin variables, the 'nuclear spin conversion' between *ortho* and *para*-H_2O is an inefficient process. Therefore, on cooling the sample to liquid helium temperatures the two spin-isomers are out of equilibrium with *ortho*-H_2O being metastable. Recently, a cryogenic NMR investigation enabled a detailed investigation of the slow conversion over a

[a] *School of Physics & Astronomy, University of Nottingham, Nottingham NG7 2RD, UK. E-mail: a.horsewill@nottingham.ac.uk*
[b] *Institut Laue–Langevin, BP 156, 38042 Grenoble, France*
[c] *School of Chemistry, University of Southampton, Southampton SO17 1BJ, UK*
[d] *Department of Chemistry, Columbia University, New York, New York 10027, USA*
[e] *Institute for Chemical Research, Kyoto University, Kyoto 611-0011, Japan*
† Deceased 24th November 2012.

period of 2 or 3 days from *ortho*-H_2O to *para*-H_2O.[17] The nuclear spin conversion was found to follow second order kinetics, demonstrating the process is bimolecular in origin and indicating neighbouring *ortho* complexes may play a role in mediating the process.

The first INS experiments on $H_2O@C_{60}$[4] were conducted on relatively impure material, leading to broad line shapes that masked important details in the spectrum. Also, in that preliminary investigation, only spectra recorded at the lowest energy transfers were available. In this new investigation we have embarked on a more in-depth INS investigation using highly purified material resulting in resolution limited line shapes. Also, higher energy transfers have been explored to provide broader insight into the quantum dynamics and the excited rotational states. Of particular topical interest is the splitting discovered by INS of the *ortho*-H_2O ground state.[4] This reveals a breaking of the icosahedral symmetry of the C_{60} cage environment and its study is expected to provide the framework for understanding the quantum dynamical properties of H_2O in a broader context. The symmetry-breaking may be fundamental to understanding other physical properties of the $H_2O@C_{60}$ system, most notably potentially fascinating dielectric properties connected with the electric dipole moment of H_2O and the interactions between the dipoles of neighbouring cages.

To induce a transition between *ortho*-H_2O and *para*-H_2O requires a simultaneous change in rotational and nuclear spin states. This is forbidden for photon spectroscopies. However, the scattering interaction between a neutron and a nucleus is mediated by spin, so *ortho* $\leftrightarrow$ *para* transitions are strongly allowed in INS. A neutron scattering investigation is therefore expected to be particularly effective in gaining insight into the fundamental characteristics of the two nuclear spin-isomers of water. Studying the INS spectrum to high energy transfers enables the eigenstates of the H_2O quantum rotor to be determined directly and the resulting acquisition of a detailed energy level diagram, including fine-structure arising from anisotropic interactions in its environment, will provide the fundamental framework for developing a future understanding of the physical properties of this supramolecular complex and its applications. This includes, for example the mechanism of nuclear spin conversion which is currently unknown and may be sensitive to the detailed proximity of neighbouring states. Furthermore, it will be important to elucidate the role of translational, or centre of mass motion of H_2O in its cage, to achieve a complete understanding of the endofullerene dynamics since the nature of the low-lying states and their dependence on the inter-cage environment may be important to the dielectric properties. Future applications relying on the energy level landscape may also exploit the entangled nature of the space and spin variables that characterise nuclear spin isomers, for example to enhance the sensitivity of NMR and magnetic resonance imaging (MRI) experiments.[18,19]

II. Theory

(i) Rotational energy levels and nuclear spin-isomers of H_2O

H_2O is an asymmetric top quantum rotor characterized by three moments of inertia $I_A > I_B > I_C$ where the subscripts label each principal axis. The moments of inertia are each defined by the geometry of the H_2O molecule and themselves define three rotational constants $A = \hbar^2/2I_A$, $B = \hbar^2/2I_B$ and $C = \hbar^2/2I_C$.

The rotational energy levels are labelled with three quantum numbers $J_{K_aK_c}$ where J relates to the total rotational angular momentum and $K_a, K_c = J, J-1, \ldots, 0$. When the symmetry of the environment is tetrahedral or higher, the degeneracy of each $J_{K_aK_c}$ level is $(2J+1)$. Lower symmetries lead to a splitting of this manifold with sub-states labelled by the quantum number $m_J \in \{-J, -J+1, \ldots, +J\}$.

The lowest energy levels $E_{JK_aK_c}$ can be approximated using expressions given by Landau and Lifshitz[20] involving the rotational constants. Using the accepted geometry of the water molecule, such calculations are found to be consistent with infrared-microwave measurements on gaseous H_2O,[21] and we find the latter provides a convenient basis for the analysis of the INS spectra of $H_2O@C_{60}$ in this paper.

The antisymmetry principle applies to systems comprising two or more indistinguishable fermions. Therefore, H_2O is a quantum rotor characterized by complete eigenfunctions, including space and spin variables, that must be antisymmetric upon exchange of identical ^1H nuclei. As a result, the Pauli Exclusion Principle (PEP) applies and only particular combinations of spatial and spin eigenfunctions are allowed, resulting in space-spin entanglement. For the ^1H isotopologue of H_2O, these symmetry requirements mean there are two nuclear spin isomers: *para*-H_2O is the ground state with total nuclear spin $I = 0$ and $K_a + K_c$ has even parity; *ortho*-H_2O is meta-stable with total nuclear spin $I = 1$ and $K_a + K_c$ has odd parity. This classification applies to the ground vibrational state. The rotational energy levels of $H_2O@C_{60}$ are sketched in Fig. 1. Here the energies of the $J = 0$ and $J = 1$ states are those determined by INS while the energies of higher rotational states are based on data for gaseous water.[21]

(ii) Inelastic neutron scattering

Incident neutrons with wavelength λ_n are scattered by the two ^1H nuclei belonging to the H_2O molecule. The energies and wave vectors of the incident and scattered neutrons are given by $(E_i, \mathbf{k}_i)$ and $(E_f, \mathbf{k}_f)$ respectively. The neutron energy (NE) transfer is $\Delta E = \hbar\omega = E_i - E_f$ and the neutron momentum transfer is $\hbar\boldsymbol{\kappa} = \hbar\mathbf{k}_i - \hbar\mathbf{k}_f$. The double differential scattering cross-section is[22–24]

$$\frac{\partial^2\sigma}{\partial\Omega\partial\omega} = \frac{\mathbf{k}_f}{\mathbf{k}_i} S(\boldsymbol{\kappa}, \omega) \tag{1}$$

where

$$S(\boldsymbol{\kappa}, \omega) = \sum_i p_i \sum_f |\langle i|V_{HH}|f\rangle|^2 \delta\left(\hbar\omega - E_i + E_f\right) \tag{2}$$

The scattering involves a scalar coupling between the neutron spin σ and a proton spin $\mathbf{I}_\alpha$. The statistical weight of the initial state is p_i. The interaction potential defining this scattering process is,

$$V_{HH} = \sum_{\alpha=1,2} e^{i\boldsymbol{\kappa}\cdot\mathbf{R}_\alpha} \left\{ b_{coh} + \frac{b_{incoh}}{2} \boldsymbol{\sigma}\cdot\mathbf{I}_\alpha \right\} \tag{3}$$

Here b_{coh} and b_{incoh} are the coherent and incoherent scattering lengths of the ^1H nucleus. The position vector of proton labelled

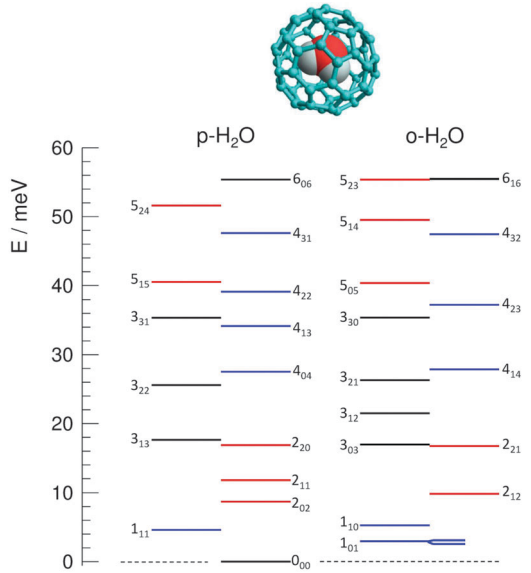

Fig. 1 The rotational energy levels of the *ortho* and *para* spin-isomers of water in the endofullerene $H_2O@C_{60}$. The states are labelled by the quantum numbers $J_{K_aK_c}$ (see text for details). The energies of the $J = 0$ and $J = 1$ states have been determined by INS while the energies of higher rotational states are based on gaseous water.[21]

$\alpha = 1, 2$ is $\mathbf{R}_\alpha = \mathbf{R}_0' + (-1)^\alpha \boldsymbol{\rho}/2$ where $\boldsymbol{\rho}$ is the inter-proton vector. The vector $\mathbf{R}_0' = \mathbf{R}_0 - \mathbf{m}$ is defined by the centre of mass vector $\mathbf{R}_0$ of the water molecule and the vector $\mathbf{m}$ defined by the perpendicular from the bisector of $\boldsymbol{\rho}$ to the centre of mass.

Evaluating the summation in eqn (3) over α, we arrive at similar expressions to the case of the H_2 molecule,[7] as follows,

$$V_{\mathrm{HH}} = \mathrm{e}^{i\boldsymbol{\kappa}\cdot\mathbf{R}_0'}\left\{V_{\mathrm{pp}}' + V_{\mathrm{oo}}' + V_{\mathrm{op}}'\right\} \quad (4)$$

where

$$V_{\mathrm{pp}}' = 2b_{\mathrm{coh}}\cos\left(\frac{1}{2}\boldsymbol{\kappa}\cdot\boldsymbol{\rho}\right) \quad (5)$$

$$V_{\mathrm{oo}}' = \frac{b_{\mathrm{incoh}}}{2}\cos\left(\frac{1}{2}\boldsymbol{\kappa}\cdot\boldsymbol{\rho}\right)\boldsymbol{\sigma}\cdot(\mathbf{I}_1 + \mathbf{I}_2) \quad (6)$$

and

$$V_{\mathrm{op}}' = i\frac{b_{\mathrm{incoh}}}{2}\sin\left(\frac{1}{2}\boldsymbol{\kappa}\cdot\boldsymbol{\rho}\right)\boldsymbol{\sigma}\cdot(\mathbf{I}_1 - \mathbf{I}_2) \quad (7)$$

The term V_{oo}' mediates transitions in which both the initial and final states are *ortho*-H_2O and where there is no change in total nuclear spin ($\mathbf{I}_1 + \mathbf{I}_2$). This term has zero probability for inducing transitions between two states of the *para* spin-isomer because *para*-H_2O has total nuclear spin zero. The term V_{op}' applies to transitions between *ortho*-H_2O and *para*-H_2O where it mediates transitions that involve a change in total nuclear spin. This is important to nuclear spin-isomers since these transitions simultaneously change space and spin parts of the wave function. The term V_{pp}' applies to transitions where both initial and final states are *para*-H_2O, however since $b_{\mathrm{coh}} \ll b_{\mathrm{incoh}}$ this only makes a very minor contribution to $S(\boldsymbol{\kappa},\omega)$.

In $H_2O@C_{60}$, the neutron scattering is dominated by ^1H because its incoherent scattering length dominates among the nuclear species in the sample. NE loss transitions characterise those in which the neutron loses energy to the sample. In such a case the NE transfer is positive, measured relative to the sample, where an H_2O rotor is promoted from a lower to a higher energy level. Conversely, in NE gain transitions the neutron gains energy when the H_2O rotor undergoes a downward transition in energy.

III. Experimental details

INS experiments were conducted using three spectrometers, IN4C, IN5 and IN1-Lagrange, installed on the high flux reactor at the Institut Laue–Langevin (ILL) in Grenoble. The instrument configurations adopted for endofullerene investigations using the two time-of-flight spectrometers, IN4C and IN5, have been described in an earlier paper.[7] The IN1-Lagrange spectrometer[25] is new to endofullerene research and will be described in more detail. The spectrometer is on the 'hot source' moderator of the ILL reactor, resulting in a high-flux beam of energetic neutrons. The incident neutron energy is determined in the primary spectrometer using single crystal monochromator crystals of Si or Cu. These are mounted in a double focusing geometrical arrangement, and in this study either Si(311) or Cu(220) Bragg reflections were selected. The neutrons scattered by the sample enter a secondary spectrometer comprising a vertical focussing reflecting surface of pyrolytic graphite analyser crystals. The design and geometry ensures only neutrons of a fixed energy (4.5 meV) are detected by a ^3He detector. A shaped beryllium filter is installed right after the sample in order to remove higher-order harmonics in the analyser reflections. To record the spectrum, the incident neutron energy was scanned by rotating the monochromator crystal enabling NE loss spectra to be measured. In this investigation the energy transfer range was confined to $12.7 \leq \Delta E \leq 80$ meV although energies beyond 300 meV have been routinely accessed in measurements on $H_2@C_{60}$.[26] The momentum transfer of detected neutrons varies systematically with NE transfer in the range $2 \leq \kappa \leq 7$ Å^{-1}. The monochromator was selected to provide the best combination of energy transfer range and resolution. The optimum energy transfer ranges selected for each monochromator were: Si(331) $12.7 < \Delta E \leq 22.5$ meV; Cu(220) $22.5 < \Delta E \leq 80$ meV. The Gaussian resolution function of the instrument depends on the monochromator and is a constant percentage of the incident neutron energy. It was determined by studying singlet transitions in the INS spectrum of $H_2@C_{60}$ as follows: FWHM (full-width half maximum): Si(311) 4.1%; Cu(220) 2.3%.

The sample of $H_2O@C_{60}$ was prepared according to published methods.[1,2] In a final stage of purification, the presence of any occluded solvent was substantially reduced by sublimation.[27] For the sample used in this investigation, approximately 90% of the C_{60} cages contained a water molecule. The powdered sample was loaded inside a rectangular Al foil sachet and mounted in the spectrometer: the IN4C and IN5 sample mass was 72 mg; the IN1-Lagrange sample mass was 62 mg. On IN1-Lagrange it was expedient to subtract background and scattering from Al and

from the C_{60} cage. This was achieved using a 'blank' sample with matching mass of empty C_{60} cages prepared in an identical Al foil sachet.

IV. Results

(i) The meta-stable *ortho*-H_2O nuclear spin isomer

The IN4C spectrum of $H_2O@C_{60}$ recorded at 1.6 K with λ_n = 3.0 Å is presented in Fig. 2. This wavelength combines high resolution with optimum neutron flux. A peak is observed in NE gain (negative energy transfer) centred on −2.56 meV. For this peak to appear at low temperature with measurable intensity is a manifestation of nuclear spin-isomerism and the meta-stability of *ortho*-H_2O. This peak originates in the transition from the ground state of *ortho*-H_2O (1_{01}) to the ground state of *para*-H_2O (0_{00}). As a result the scattered neutron gains energy from the encounter with the entrapped H_2O molecule in its *ortho* spin isomer state.

The intensity of this NE gain peak is observed to diminish with time after cooling to 1.6 K. In Fig. 2, IN4C spectra (λ_n = 3.0 Å) are presented that were recorded, (a) during the 1st hour following initial cooling to 1.6 K (red) and during a one hour period that began 7 hours 20 minutes after initial cooling (blue), and (b) the sum of scattered neutrons recorded during an 8 h 20 m period after cooling. The observed decay in the intensity of the NE gain peak reveals the slow conversion from meta-stable *ortho*-H_2O (1_{01}) to *para*-H_2O (0_{00}). During the same 8.3 hour period, a prominent doublet in NE loss centred on $\Delta E \approx +2.7$ meV is observed to increase in intensity. This growth indicates that the doublet predominately arises from transitions originating in the *para*-H_2O nuclear spin isomer. A more detailed analysis of the INS peak intensities as a function of time provides deeper insight into the kinetics of spin-isomer conversion,[17] however these details will be the subject of a future publication.

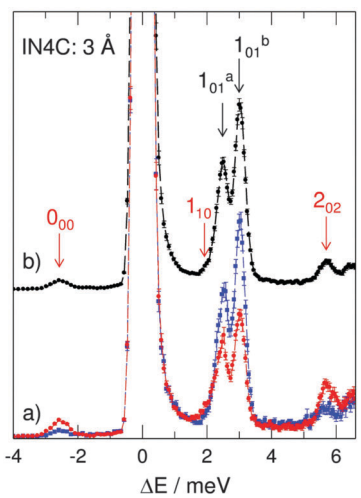

Fig. 2 The INS spectrum of $H_2O@C_{60}$ recorded at 1.6 K on IN4C (λ_n = 3 Å): (a) spectrum recorded in the first hour (red) and 8th hour (blue) after cooling; (b) the sum of all neutrons recorded during a period of 8.3 hours after cooling. The labels identify the final states of the transitions: transitions originating in 1_{01} (red text); transitions originating in 0_{00} (black text).

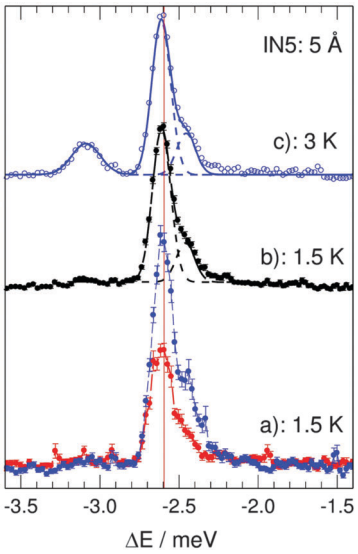

Fig. 3 The INS spectrum of $H_2O@C_{60}$ recorded at 1.5 K on IN5 (λ_n = 5 Å): (a) spectrum recorded in the 1st hour (red) and 5th hour (blue) after cooling; (b) the sum of all neutrons recorded during a period of 5 hours after cooling; (c) the sum of scattered neutrons recorded during 3 hours after cooling to 3 K. The spectra reveal the splitting of the 1_{01} state *ortho*-water state arising from a symmetry breaking interaction.

The NE gain spectrum has been studied with higher resolution on IN5 (λ_n = 5 Å). In Fig. 3 IN5 spectra are shown, recorded at 1.5 K and 3 K. The time dependence is again recorded, showing (a) the 1.5 K spectrum recorded during the 1st hour (red) and the 5th hour (blue) after cooling, (b) the sum of scattered neutrons recorded during 5 hours after initial cooling to 1.5 K, (c) the sum of scattered neutrons recorded during 3 hours after cooling to 3 K. As on IN4C, conversion from *ortho* to *para*-H_2O is revealed in the decay in intensity of the −2.56 meV peak with time after cooling to 1.5 K. However, with the increased resolution a shoulder is resolved on IN5, showing most prominently in the summed spectrum Fig. 3b which has the best neutron counting statistics. The IN5 spectrum at 1.5 K therefore comprises a peak with energy transfer −2.61 meV and a shoulder centred on −2.46 meV. The best fit components are shown with dashed lines in Fig. 3 and the intensity weighted mean energy transfer agrees well with the NE gain peak measured at 1.6 K with lower resolution on IN4, Fig. 2.

Raising the temperature to 3 K reveals the growth of a new NE gain peak centred on −3.09 meV, Fig. 3c. This highlights a splitting of the 1_{01} *ortho* ground state. This has been studied in detail in a series of spectra recorded at higher temperature, Fig. 4. In these experiments, before each run the sample was systematically prepared by warming the sample to $T > 40$ K for 50 minutes where equilibrium was restored between the two spin-isomers, replenishing the population of the *ortho*-H_2O state. Then the sample was rapidly cooled to the required temperature whereupon the IN5 spectrum was recorded over a 3 hour period. Spectra recorded in the temperature range $1.5 \leq T \leq 20.0$ K are shown in Fig. 4. Even with the small increase in temperature from 1.5 to 3.0 K, the spectrum evolves

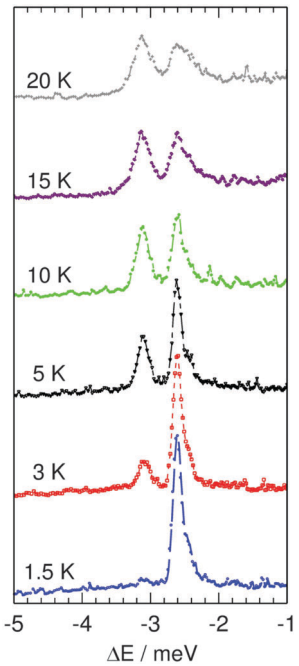

Fig. 4 INS spectra of $H_2O@C_{60}$ recorded on IN5 (λ_n = 5 Å) during 3 hours after cooling to: 1.5 K; 3.0 K; 5.0 K; 10.0 K; 15 K; 20 K.

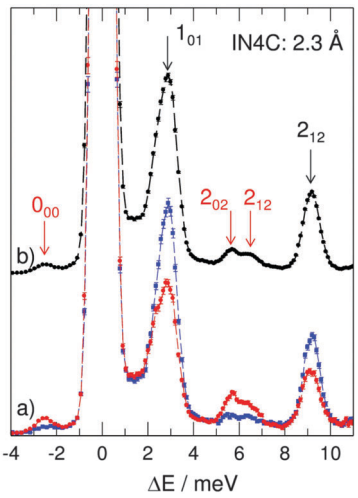

Fig. 5 The INS spectrum of $H_2O@C_{60}$ recorded at 1.6 K on IN4C (λ_n = 2.3 Å): (a) spectrum recorded in the first hour (red) and 8th hour (blue) after cooling; (b) the sum of all neutrons recorded during a period of 8 hours after cooling. The labels identify the final states of the transitions: transitions originating in 1_{01} (red text); transitions originating in 0_{00} (black text).

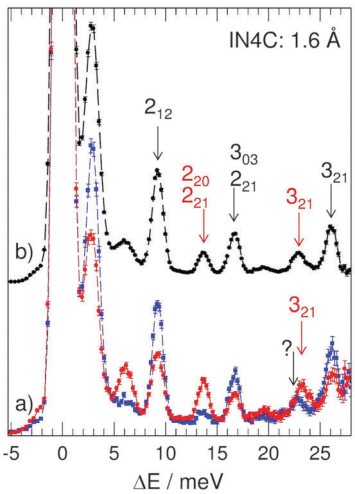

Fig. 6 The INS spectrum of $H_2O@C_{60}$ recorded at 1.6 K on IN4C (λ_n = 1.6 Å): (a) spectrum recorded in the first hour (red) and 8th hour (blue) after cooling; (b) the sum of all neutrons recorded during a period of 8 hours after cooling. The labels identify the final states of the transitions: transitions originating in 1_{01} (red text); transitions originating in 0_{00} (black text).

significantly, revealing the rapid growth of the new peak centred on −3.09 meV. This provides conclusive evidence for a splitting of the ground *ortho*-H_2O 1_{01} state confirming an earlier finding reported in.[4] However in these new experiments, with the improved sample purity that arises from sublimation, the intrinsic linewidth of the peaks in the spectrum is much narrower, enabling the splitting to be fully resolved and facilitating its study in more detail. All peaks observed in Fig. 3 and 4 arise from $1_{01} \rightarrow 0_{00}$ transitions. The splittings show the three-fold degeneracy of the 1_{01} state is raised resulting in substates $1_{01}{}^{a}$ (2.61 ± 0.05 meV), $1_{01}{}^{b}$ (3.09 ± 0.05 meV) and $1_{01}{}^{a'}$ (2.46 ± 0.05 meV). Here the specified energies are relative to 0_{00}. The raising of the degeneracy in this way reveals a symmetry breaking in the environment. More detailed analysis of the spectra in Fig. 4 will be undertaken in Section V where the insights gained will be discussed.

(ii) Higher energy excitations

Measurements extending to higher energy transfer on the NE loss side have been made using IN4C and IN1-Lagrange. In Fig. 5 and 6, IN4C spectra are displayed, recorded at 1.6 K with λ_n = 2.3 and 1.6 Å respectively. In Fig. 7, IN1-Lagrange spectra are displayed recorded at 2.5 K.

In Fig. 2, 5 and 6, three IN4C spectra are presented. The different incident wavelengths provide different energy transfer ranges. The energy resolution diminishes with decreasing wavelength. The curves in black represent a sum of all neutrons detected during a period of 8 hours after initial cooling. The curves in red are the spectra recorded during the first hour after cooling and the curves in blue are the spectra recorded during the 8th hour after cooling.

In Fig. 7, three IN1-Lagrange spectra are recorded, extending the study to energy transfers of 80 meV. Immediately following the initial cool-down, the sample is a mixture of *ortho* and *para*-H_2O. A spectrum representative of such a mixture is shown in red, recorded as a sum of scattered neutrons during the first 3 hours after cooling. The spectrum in blue was recorded during a 5 hour period beginning 18 hours after the sample was cooled to 2.5 K. By this time the sample has substantially converted to *para*-H_2O[17] and is labelled as such. The spectrum in black is a difference spectrum of the two, representing the spectrum of *ortho*-H_2O.

Significantly, as the spectra recorded on the three spectrometers reveal, the spin-isomer conversion of the sample provides

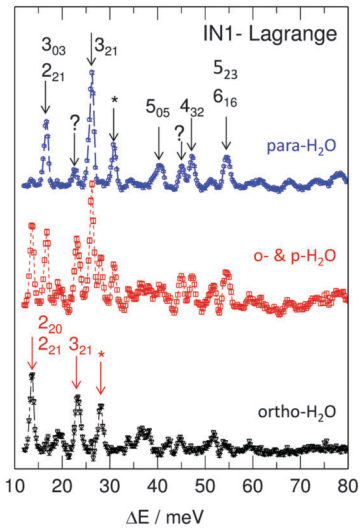

Fig. 7 INS spectra of $H_2O@C_{60}$ recorded at 2.5 K on IN1-Lagrange: (blue) the spectrum of *para*-H_2O recorded during a 5 hour period beginning 18 hours after initial cooling to 2.5 K, allowing the sample to convert to the *para* ground state; (red) the spectrum recorded during the first 3 hours after cooling to 2.5 K, representing a mixture of *ortho* and *para*-H_2O; (black) the difference spectrum representing predominantly *ortho*-H_2O. The labels identify the final states of the transitions: transitions originating in 1_{01} (red text); transitions originating in 0_{00} (black text). Two unassigned peaks involving the same final state are identified with an asterisk (see text for details).

a very convenient device for conclusively identifying the initial state associated with particular peaks in the INS spectrum. Therefore those peaks that grow with time have *para*-H_2O as an initial state, whereas those peaks that decay with time originate in *ortho*-H_2O. Moreover, at low temperature (1.5–2.5 K) the rotational energy level separations are large compared with k_BT, so in the INS spectra there are only two possible initial states, namely the ground states of *ortho*- and *para*-H_2O.

The analysis of the INS spectra will be discussed in the next section.

V. Discussion

(i) The rotational spectrum of $H_2O@C_{60}$

As with INS spectra of H_2, transitions between two states of *para*-H_2O have negligibly small intensity at the levels of sensitivity attained in this investigation. Therefore the INS spectrum is dominated by *ortho* ↔ *para* and *ortho* ↔ *ortho* transitions. Unlike earlier investigations of $H_2@C_{60}$ which does not exhibit nuclear spin conversion,[5,7,8] the sample of $H_2O@C_{60}$ spontaneously converts from *ortho*-H_2O to *para*-H_2O over a period of many hours providing an important tool in assigning INS peaks to transitions among the energy levels of $H_2O@C_{60}$. To further assist the assignments, a good basis for a provisional energy level diagram, Fig. 1, is provided by the infrared-microwave spectrum of gaseous H_2O.[21] The assignments of the observed INS peaks are presented in Table 1. They are also labelled on the respective INS spectra, Fig. 2 to 7, where black lettering indicates the final state of a transition originating in the 0_{00} ground state of *para*-H_2O and red lettering identifies the final state of a transition originating in the 1_{01} ground state of *ortho*-H_2O.

Table 1 Assignments for rotational transitions in the INS spectra of $H_2O@C_{60}$

Instrument	meV	Transition
para spectrum		
IN4C 3 Å	2.50 ± 0.05	$0_{00} \rightarrow 1_{01}{}^{a}$
IN4C 3 Å	3.02 ± 0.05	$0_{00} \rightarrow 1_{01}{}^{b}$
IN4C 1.6 & 2.3 Å	9.20 ± 0.05	$0_{00} \rightarrow 2_{12}$
Lagrange & IN4C	16.6 ± 0.1	$0_{00} \rightarrow 2_{21}\ 3_{03}$
Lagrange & IN4C	22.8 ± 0.1	$0_{00} \rightarrow$?
Lagrange & IN4C	26.1 ± 0.2	$0_{00} \rightarrow 3_{21}$
Lagrange	30.8 ± 0.2	$0_{00} \rightarrow$ *
Lagrange	39.4 ± 0.2	$0_{00} \rightarrow$?
Lagrange	40.7 ± 0.2	$0_{00} \rightarrow 5_{05}$
Lagrange	45.1 ± 0.2	$0_{00} \rightarrow$?
Lagrange	47.3 ± 0.2	$0_{00} \rightarrow 4_{32}$
Lagrange	54.6 ± 0.2	$0_{00} \rightarrow 5_{23}\ 6_{16}$
ortho spectrum		
IN4C 3 Å	−2.56 ± 0.05	$1_{01}{}^{a,a'} \rightarrow 0_{00}$
IN5	−2.46 ± 0.05	$1_{01}{}^{a'} \rightarrow 0_{00}$
IN5	−2.61 ± 0.05	$1_{01}{}^{a} \rightarrow 0_{00}$
IN5	−3.09 ± 0.05	$1_{01}{}^{b} \rightarrow 0_{00}$
IN4 3 Å	2.1 ± 0.1	$1_{01}{}^{a} \rightarrow 1_{11}$
IN4C 2.3 Å	5.68 ± 0.05	$1_{01} \rightarrow 2_{02}$
IN4C 2.3 Å	6.51 ± 0.05	$1_{01} \rightarrow 2_{12}$
Lagrange & IN4C	13.7 ± 0.1	$1_{01} \rightarrow 2_{20}\ 2_{21}\ 3_{03}$
Lagrange & IN4C	23.3 ± 0.2	$1_{01} \rightarrow 3_{21}$
Lagrange	28.1 ± 0.2	$1_{01} \rightarrow$ *

Earlier, the splitting of the 1_{01} ground state of *ortho*-H_2O was established, revealing itself in the NE gain and NE loss transitions $1_{01}{}^{a,b,a'} \leftrightarrow 0_{00}$ recorded on IN4C and IN5, Fig. 2–4. In the same low energy transfer region, Fig. 2, we identify a NE loss transition which is just resolved as a small shoulder at 2.1 ± 0.1 meV on the low energy side of the 1_{01} doublet. It identifies itself as originating in *ortho*-H_2O by its diminishing intensity with time, appearing on the side of the larger '*para*' peak that grows with time. At 1.6 K only the lowest energy component of *ortho*-H_2O, $1_{01}{}^{a}$, is populated, so we conclude the final state energy relating to this shoulder is 4.74 meV relative to 0_{00}. Within experimental uncertainties, this matches the energy of the 1_{11} state in gaseous H_2O, so we conclude the shoulder is $1_{01}{}^{a} \rightarrow 1_{11}$. We similarly conclude the neighbouring transition $1_{01}{}^{a} \rightarrow 1_{10}$ would appear at approximately +2.6 meV, which lies beneath the $0_{00} \rightarrow 1_{01}$ peaks and therefore cannot be separately resolved.

The first components of the $J = 2$ multiplet are observed in Fig. 5, where the shorter neutron wavelength configuration of IN4C, $\lambda_n = 2.3$ Å, provides access to higher energies, albeit with lower resolution. In this spectrum the 2_{12} state is observed in transitions that originate in both 0_{00} and $1_{01}{}^{a}$. Within experimental uncertainties, the energy transfer difference between the two, 2.69 meV, corresponds closely to the measured energy of $1_{01}{}^{a}$, providing a further, but less direct example of where the splitting of 1_{01} is detailed in the spectrum.

Still higher energy states are identified in Fig. 6 (IN4C) and 7 (IN1-Lagrange). Analogous to the 2_{12} state described above, the 3_{21} state is observed in transitions originating in 0_{00} and 1_{01}.

Of the two sets of data, for this $J = 3$ state the best resolution is achieved on IN1-Lagrange and the energy transfers reported in Table 1 arise from fitting to this spectrum. The energy difference between $3_{21} \rightarrow 0_{00}$ and $3_{21} \rightarrow 1_{01}$ is 2.85 meV, which is slightly larger than the analogous example relating to the 2_{12} state above. However, unlike the IN4C spectrum, at the slightly elevated temperature of the IN1-Lagrange spectrum, 2.5 K, both $1_{01}{}^{a}$ and $1_{01}{}^{b}$ are populated and as a result the observed energy difference corresponds closely to the mean energy of the states $1_{01}{}^{a}$ and $1_{01}{}^{b}$. Therefore, the two examples of transitions involving 2_{12} and 3_{21} together provide a picture fully consistent with the properties of the 1_{01} state elucidated from the IN5 spectra.

For a fully converted sample, the peaks in the INS spectrum arise solely from 0_{00}. Therefore, given only *para–ortho* transitions can arise, the '*para* spectrum', Fig. 7, provides a direct mapping of the energy levels of *ortho*-H_2O. Where there is a close correspondence with the energies of states identified in gaseous H_2O, these peaks are assigned accordingly. However, with increasing energy transfer the absolute resolution diminishes so assignments become increasingly ambiguous beyond $\Delta E = 30$ meV.

For transitions originating in *ortho*-H_2O (1_{01}), the final state can be either *para* or *ortho*-H_2O, so in general the '*ortho* spectrum' is expected to contain twice the density of final states as the '*para* spectrum', increasing the scope for overlapping peaks. Indeed this influences the information content of the *ortho* spectrum in Fig. 7. This is a difference spectrum, so the doubling of the peak density combines with the inferior neutron counting statistics to provide little discernible detail above 30 meV. This is compounded by the diminishing absolute resolution at the higher energies.

Not all rotational energy levels within range have been identified in the spectra, indicating that some INS transitions may have low intensity. Although it is commonly stated that INS spectra 'have no selection rules',[28] in the study of quantum rotors it transpires angular momentum has a significant role to play, with the capacity to introduce selection rules into the description. Indeed, in the endofullerene $H_2@C_{60}$, selection rules were identified rendering certain transitions forbidden.[29] The INS peak intensities are determined by the matrix element $\langle i|V_{HH}|f\rangle$, eqn (2)–(7); some transitions may have weak intensity, others may conceivably be forbidden. However to achieve a quantitative understanding as it applies to $H_2O@C_{60}$, requires computational investigations of the C_{60} cage potential from which the wave functions of the entrapped H_2O molecules required to evaluate the matrix element can be determined. This is beyond the scope of this experimental investigation but the results presented will inform future computational and theoretical studies.

(ii) Symmetry breaking revealed in the ground state of the *ortho*-H_2O spin isomer

The IN5 spectra of Fig. 4 and 5 reveal the splitting of the 1_{01} state. The spectra are dominated by two peaks with energy transfer −2.61 and −3.09 meV. The latter is almost absent at 1.5 K, but grows rapidly with increasing temperature. Raising the temperature to just 3 K is sufficient to populate this state. In addition there is a small shoulder at −2.46 meV on the side of the −2.61 meV peak. An analysis of the temperature dependence data provides the necessary insight to formulate a model.

At $T < 10$ K, the IN5 spectra contain just the three components identified above. Good fits are obtained using three Gaussian functions. The two lowest energy features at −2.61 and −2.46 meV have FWHM equal to the IN5 resolution function. However, the −3.09 meV peak is approximately 40% broader indicating the presence of unresolved structure. We may tentatively associate this excess width with the presence of the −2.46 meV shoulder on the side of the −2.61 meV peak. This suggests, in addition to a main symmetry breaking interaction that splits $1_{01}{}^{a}$ and $1_{01}{}^{b}$, there are additional inhomogeneities responsible for the shoulder at −2.46 meV and the excess width of the −3.09 meV peak.

With increasing temperature, excited states of *para*-H_2O and *ortho*-H_2O become populated leading to an apparent broadening of the peaks as additional NE gain transitions appear in this energy transfer window. Therefore, to gain fully quantitative insight from the peak intensities it is necessary to include five additional transitions in the fitting model for $T \geq 15$ K. Their peak positions are defined by the energy level model, Fig. 1. Constraining all peak positions to their measured or inferred energies, least square fits have been made to the spectra in Fig. 5 using Gaussians. All peaks have FWHM equal to the resolution function, except the peak at −3.09 meV which has FWHM equal to that measured at 3 K. In the fitting model, the only variables are the peak intensities. From this analysis the integrated intensities of the −2.61, −3.08 and −2.46 meV peaks have been determined and plotted in Fig. 8.

The intensity of the −2.61 meV peak is observed to diminish rapidly with increasing temperature, reducing by a factor

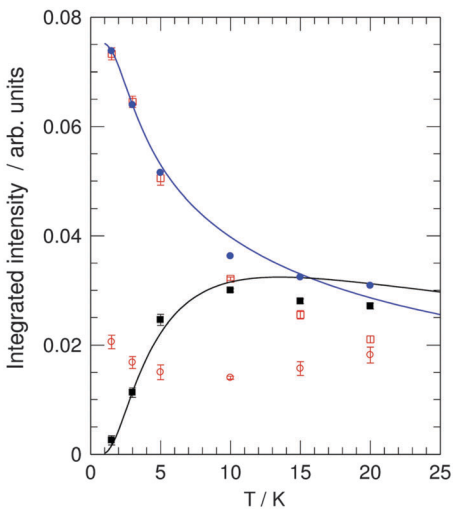

Fig. 8 The integrated intensities of the INS peaks recorded on IN5 (Fig. 5). Open red squares: $1_{01}{}^{a} \rightarrow 0_{00}$ (−3.09 meV). Filled black squares: $1_{01}{}^{b} \rightarrow 0_{00}$ (−2.61 meV). Open red circles: $1_{01}{}^{a'} \rightarrow 0_{00}$ (−2.46 meV). Filled blue circles: the sum of $1_{01}{}^{a} \rightarrow 0_{00}$ and $1_{01}{}^{a'} \rightarrow 0_{00}$. Solid lines (scaled to data): blue, the Boltzmann population of the $1_{01}{}^{a}$ state; black, the Boltzmann population of the $1_{01}{}^{b}$ state.

approximately two in the range $1.5 \leq T \leq 10$ K. In the same temperature range the −3.09 meV peak grows until by 10 K it has almost equal intensity with that of the −2.61 meV peak. The intensity of the −2.46 meV shoulder displays much weaker temperature dependence. In Fig. 8, the solid lines are the calculated Boltzmann populations representing the statistical weight p_i of the relevant initial state, eqn (2). These have been uniformly scaled for comparison with the data using the integrated intensity of the −2.65 meV peak at $T = 1.5$ K as the reference. The Boltzmann populations have been calculated in a model defining the energies and degeneracies of the 39 lowest energy rotational states. The energies of the $J = 0$ and $J = 1$ rotational states are those measured by INS, while the energies of higher rotational states are those of gaseous water.[21] The model assumes there is no equilibrium between the *ortho* and *para*-H_2O states, but there is equilibrium between states of the same spin-isomer species. The agreement with experiment has been achieved by assuming the ground *ortho* state is split into the lowest energy $1_{01}{}^{a}$ state with degeneracy $g = 2$ and a higher energy $1_{01}{}^{b}$ state with degeneracy $g = 1$.

Fig. 8 shows good agreement between the integrated peak intensities and the calculated Boltzmann populations. The modelled rise in intensity of the −3.09 meV peak appears at exactly the observed temperature and the shape of the curve shows very good agreement with experiment. The experimental and calculated curves in Fig. 8 provide confirmation that the *ortho* ground state is split into its two states, $1_{01}{}^{a}$ and $1_{01}{}^{b}$ with degeneracies 2 and 1 respectively. This characterises the principle symmetry-breaking interaction.

In an environment with high symmetry, the predicted degeneracy of the 1_{01} state is $g = 3$. Therefore, with two principle peaks exhibiting degeneracies of 2 and 1 respectively, the question arises of the nature of the −2.46 meV shoulder labelled $1_{01}{}^{a'}$. Summing the integrated intensities of the −2.65 and −2.46 meV peaks together (filled blue circles, Fig. 8), provides a set of data that displays closer agreement with the calculated Boltzmann population of the $1_{01}{}^{a}$ state. Therefore, we conclude the $1_{01}{}^{a'}$ shoulder is intimately connected with $1_{01}{}^{a}$ and that this feature is a similar manifestation to the excess width of the −3.09 meV peak.

What is the nature of the symmetry breaking interaction that gives rise to the 1_{01} splittings? Two possibilities seem to arise. The first alternative suggests a property of an individual endofullerene where there is a spontaneous Jahn–Teller-like symmetry breaking arising from interactions of the H_2O molecule with its cage. A second alternative is that the symmetry breaking arises from inter-molecular interactions between neighbouring $H_2O@C_{60}$ molecules, possibly mediated by interactions between the electric dipole moments of the H_2O molecules. Either could form a theoretical basis for the principle symmetry-breaking splitting into $1_{01}{}^{a}$ and $1_{01}{}^{b}$. The smaller splitting exhibited by the $1_{01}{}^{a'}$ shoulder at −2.46 meV, coupled with the excess width of the −3.09 meV peak, is consistent with an interaction of the second kind, possibly relating to inhomogeneities arising from the small percentage (approximately 10%) of C_{60} cages that have no water molecule present.

(iii) Fine structure of the rotational spectrum

To facilitate a complete analysis of the INS spectra the observed splitting of the 1_{01} *ortho*-H_2O ground state has a number of implications that must be addressed. We have earlier seen how the splitting of the *ortho*-H_2O ground state can influence the precise energies of the INS peaks in the spectrum. For example, in an INS spectrum recorded at 1.5 K, the peak energies are referenced to $1_{01}{}^{a}$ whereas in a spectrum recorded at 2.5 K the peak energies are referenced to the centre of the 1_{01} band. However, the effects of symmetry breaking will not be confined to the ground rotational state. The same process is expected to raise the $(2J + 1)$ degeneracy generally, splitting all excited rotational states and resulting in fine structure in the INS spectrum.

On close inspection, a number of peaks observed in the IN1-Lagrange spectra are broader than the resolution function and asymmetric in shape, indicating the presence of unresolved structure. However, a complete analysis of this effect is currently premature. To unambiguously make assignments will require further theoretical investigations, including a complete description of the cage potential, incorporating a model for the influence of any symmetry breaking interaction on the dynamical eigenstates of H_2O and a simulation of the INS peak intensities. For the present, where nascent structure is suspected resulting in asymmetric peaks, the energies of the assigned transitions reported in Table 1 have been determined as the intensity weighted mean.

(iv) Translational modes

Hitherto the emphasis has been on the rotational dynamics about the centre of mass. We have not addressed the issue of the translational modes arising from centre of mass displacements of H_2O inside its cage. In $H_2@C_{60}$ the first translational mode was observed centred on 22.5 meV.[5,7,8] In a simple analysis based on a harmonic cage potential, the translational energies scale inversely with the square root of the reduced mass of the entrapped particle. Therefore, in the case of H_2O and H_2 the simple scaling factor is 3, crudely predicting a translational energy of 7.5 meV for $H_2O@C_{60}$. However, the confining potential is determined by non-bonding interactions between the entrapped molecule and the C_{60} cage and is expected to be significantly different for H_2O and H_2. Therefore simple scaling principles are inadequate.

In an experimental approach, unambiguous signatures in the INS spectrum are required to make any assignment. A number of observed peaks fail to follow the pattern exhibited by pure rotations in gaseous H_2O. Notably, consider the 30.8 meV peak identified with an asterisk in the *para* spectrum of Fig. 7. This transition must originate in 0_{00} and have a final state that resides in *ortho*-H_2O. However, the two closest *para* → *ortho* transitions predicted by the rotational energy levels of gaseous H_2O differ by energies +2.9 and −4.6 meV respectively, significantly larger than experimental uncertainties. Similarly, a peak with energy transfer 28.1 meV observed in the *ortho* spectrum (asterisk Fig. 7) must originate in 1_{01}. Its energy is offset by more

than ±3 meV from any *ortho* → *ortho* or *ortho* → *para* rotational transition predicted for gaseous H_2O. Significantly, the difference in the observed energies of the 30.8 and 28.1 meV peaks is close to the mean energy of the 1_{01} doublet, leading us to conclude they share the same final state. The discrepancy in energy of this unknown final state from any rotational state of gaseous H_2O is large compared to the observed splitting of the 1_{01} state, so the symmetry breaking interaction probably does not provide the basis for explaining the observations. However, the option remains open that the unassigned peaks could involve a translational mode of H_2O inside its cage. Currently there is no information on the cage potential but allowing for the increased mass of H_2O and applying simple principles based on a harmonic potential, it seems unlikely this unassigned final state could be the first translational mode. That would require a substantially narrower cage potential for $H_2O@C_{60}$ compared with $H_2@C_{60}$. Nevertheless, the mode could relate to a higher translational harmonic, or a combined translation–rotation transition. To resolve these questions will require quantum chemical calculations of the cage potential, where the influence of the symmetry-breaking interaction must also be factored in.

VI. Concluding remarks

The small molecule endofullerenes provide well characterized systems with narrow, resolution limited peaks in the INS spectrum. As with earlier studies on entrapped H_2,[5,7,8] this study of $H_2O@C_{60}$ emphasises the importance of INS investigations in the study of quantum rotors. With its ability to induce transitions between *ortho* and *para* species, the technique is shown to be particularly effective in the study of nuclear spin-isomerism. Using a combination of INS spectrometers with different energy transfer ranges enables the dynamical states of an entrapped quantum rotor to be successfully determined with good resolution. As a result, the $H_2O@C_{60}$ system provides a unique opportunity to study isolated water molecules in a symmetrical 'nanolaboratory' environment and for the *ortho*-H_2O and *para*-H_2O species to be uniquely identified. As a result, a splitting of the *ortho*-H_2O ground state has been identified pointing to a symmetry-breaking interaction acting on the H_2O molecules in their C_{60} cages. A quantitative analysis of the temperature dependence of this spectrum has corroborated this interpretation, providing deeper insight.

While many of the low-lying levels can be accurately determined simply on the basis of the experimental data, deeper insight into the excited states of the rotational spectrum must await a high-quality computational investigation, for example of the kind pioneered by Bačić and Xu.[29–32] Similarly the nature of the translational states of the entrapped water molecule is a topic that requires advanced theoretical and computational studies to be conducted to quantify the cage potential.

Much more so than in $H_2@C_{60}$, the *ortho* ground state of $H_2O@C_{60}$ is shown to be sensitive to the molecular environment external to the fullerene cage. For the $H_2O@C_{60}$ complex this is clear in two ways; (1) the ground *ortho* state is split; (2) there is a strong line-broadening effect due to the presence of occluded solvent impurities;[4] (3) inhomogeneities in the inter-fullerene environment have been revealed in the line-shapes of the peaks in the NE gain spectrum. By contrast, the INS spectrum of $H_2@C_{60}$ is much more representative of an isolated endofullerene cage, exhibiting no substantial sign within the spectrometer resolution of a splitting of the ground *ortho*-H_2 state, or sensitivity to sample purity.[5,7,8] This difference between the behaviour of H_2O and H_2 guest molecules may be attributed to the presence of a permanent electric dipole moment on the water molecule. Therefore, the nature of the inter-cage interactions and the observed symmetry breaking is a topic of considerable interest, not only to the energy level structure of the H_2O molecules but also to the more macroscopic dielectric properties of water based endofullerenes.

Acknowledgements

The endofullerene research programme is supported in the UK by the Engineering and Physical Sciences Research Council, including support to KG in the form of a postgraduate scholarship. The authors at Columbia University thank the NSF for its generous support through Grant No. CHE 07 17518.

References

1 K. Kurotobi and Y. Murata, *Science*, 2011, **333**, 613–616.
2 K. Komatsu, M. Murata and Y. Murata, *Science*, 2005, **307**, 238–240.
3 M. H. Levitt and A. J. Horsewill, *Philos. Trans. R. Soc., A*, 2013, **371**, 20130124.
4 C. Beduz, M. Carravetta, J. Y. C. Chen, M. Concistre, M. Denning, M. Frunzi, A. J. Horsewill, O. G. Johannessen, R. Lawler, X. Lei, M. H. Levitt, Y. Li, S. Mamone, Y. Murata, U. Nagel, T. Nishida, J. Ollivier, S. Rols, T. Room, R. Sarkar, N. J. Turro and Y. Yang, *Proc. Natl. Acad. Sci. U. S. A.*, 2012, **109**, 12894–12898.
5 A. J. Horsewill, K. Goh, S. Rols, J. Ollivier, M. R. Johnson, M. H. Levitt, M. Carravetta, S. Mamone, Y. Murata, J. Y. C. Chen, J. A. Johnson, X. Lei and N. J. Turro, *Philos. Trans. R. Soc., A*, 2013, **371**, 20110627.
6 A. J. Horsewill, K. S. Panesar, S. Rols, M. R. Johnson, Y. Murata, K. Komatsu, S. Mamone, A. Danquigny, F. Cuda, S. Maltsev, M. C. Grossel, M. Carravetta and M. H. Levitt, *Phys. Rev. Lett.*, 2009, **102**, 013001.
7 A. J. Horsewill, K. S. Panesar, S. Rols, J. Ollivier, M. R. Johnson, M. Carravetta, S. Mamone, M. H. Levitt, Y. Murata, K. Komatsu, J. Y. C. Chen, J. A. Johnson, X. Lei and N. J. Turro, *Phys. Rev. B: Condens. Matter Mater. Phys.*, 2012, **85**, 205440.
8 A. J. Horsewill, S. Rols, M. R. Johnson, Y. Murata, M. Murata, K. Komatsu, M. Carravetta, S. Mamone, M. H. Levitt, J. Y. C. Chen, J. A. Johnson, X. Lei and N. J. Turro, *Phys. Rev. B: Condens. Matter Mater. Phys.*, 2010, **82**, 081410.

9 S. Mamone, J. Y. C. Chen, R. Bhattacharyya, M. H. Levitt, R. G. Lawler, A. J. Horsewill, T. Room, Z. Bačić and N. J. Turro, *Coord. Chem. Rev.*, 2011, **255**, 938–948.

10 M. Carravetta, O. G. Johannessen, M. H. Levitt, I. Heinmaa, R. Stern, A. Samoson, A. J. Horsewill, Y. Murata and K. Komatsu, *J. Chem. Phys.*, 2006, **124**, 104507.

11 M. Carravetta, A. Danquigny, S. Mamone, F. Cuda, O. G. Johannessen, I. Heinmaa, K. Panesar, R. Stern, M. C. Grossel, A. J. Horsewill, A. Samoson, M. Murata, Y. Murata, K. Komatsu and M. H. Levitt, *Phys. Chem. Chem. Phys.*, 2007, **9**, 4879–4894.

12 S. Mamone, M. Concistre, I. Heinmaa, M. Carravetta, I. Kuprov, G. Wall, M. Denning, X. Lei, J. Y. C. Chen, Y. Li, Y. Murata, N. J. Turro and M. H. Levitt, *ChemPhysChem*, 2013, **14**, 3121–3130.

13 M. Ge, U. Nagel, D. Huevonen, T. Room, S. Mamone, M. H. Levitt, M. Carravetta, Y. Murata, K. Komatsu, J. Y. C. Chen and N. J. Turro, *J. Chem. Phys.*, 2011, **134**, 054507.

14 T. Room, L. Peedu, M. Ge, D. Huevonen, U. Nagel, S. Ye, M. Xu, Z. Bačić, S. Mamone, M. H. Levitt, M. Carravetta, J. Y. C. Chen, X. Lei, N. J. Turro, Y. Murata and K. Komatsu, *Philos. Trans. R. Soc., A*, 2013, **371**, 20110631.

15 M. Ge, U. Nagel, D. Huevonen, T. Room, S. Mamone, M. H. Levitt, M. Carravetta, Y. Murata, K. Komatsu, X. Lei and N. J. Turro, *J. Chem. Phys.*, 2011, **135**, 114511.

16 Y. Kohama, T. Rachi, J. Jing, Z. Li, J. Tang, R. Kumashiro, S. Izumisawa, H. Kawaji, T. Atake, H. Sawa, Y. Murata, K. Komatsu and K. Tanigaki, *Phys. Rev. Lett.*, 2009, **103**, 073001.

17 S. Mamone, M. Concistre, E. Carignani, B. Meier, A. Krachmalnicoff, O. G. Johannessen, X. Lei, Y. Li, M. Denning, M. Carravetta, K. Goh, A. J. Horsewill, R. J. Whitby and M. H. Levitt, *J. Chem. Phys.*, 2014, **140**, 194306.

18 T. Kravchuk, M. Reznikov, P. Tichonov, N. Avidor, Y. Meir, A. Bekkerman and G. Alexandrowicz, *Science*, 2011, **331**, 319–321.

19 V. I. Tikhonov and A. A. Volkov, *Science*, 2002, **296**, 2363.

20 L. D. Landau and E. M. Lifshitz, *Quantum Mechanics: Non-relativistic Theory*, Pergamon Press, Oxford, 3rd edn, 1977.

21 P. Helminger and F. C. Delucia, *J. Mol. Spectrosc.*, 1978, **70**, 263–269.

22 T. Yildirim and A. B. Harris, *Phys. Rev. B: Condens. Matter Mater. Phys.*, 2002, **66**, 214301.

23 R. J. Elliott and W. M. Hartmann, *Proc. Phys. Soc., London*, 1967, **90**, 671.

24 J. A. Young and J. U. Koppel, *Phys. Rev.*, 1964, **135**, A603.

25 A. Ivanov, M. Jiménez-Ruiz and J. Kulda, *J. Phys.: Conf. Ser.*, 2014, in press.

26 S. Y. Minzhong Xu, Z. Bačić, M. R. Johnson, M. Jimenez-Ruiz, S. Mamone, M. H. Levitt and A. J. Horsewill, unpublished work.

27 A. Krachmalnicoff, M. H. Levitt and R. J. Whitby, unpublished work.

28 S. F. Parker and P. I. Haris, *Spectrosc. Int. J.*, 2008, **22**, 297–307.

29 M. Xu, S. Ye, A. Powers, R. Lawler, N. J. Turro and Z. Bačić, *J. Chem. Phys.*, 2013, **139**, 064309.

30 M. Xu and Z. Bačić, *Phys. Rev. B: Condens. Matter Mater. Phys.*, 2011, **84**, 195445.

31 M. Xu, L. Ulivi, M. Celli, D. Colognesi and Z. Bačić, *Chem. Phys. Lett.*, 2013, **563**, 1–8.

32 M. Xu, F. Sebastianelli, Z. Bačić, R. Lawler and N. J. Turro, *J. Chem. Phys.*, 2008, **129**, 064313.